Technology Maturation of Active Precision Navigation for Lunar Landing

Bryan Friia[1], Aditya Mahajan[2], Michael Forrest[3], and Stefan Bieniawski[4]
Blue Origin, Kent, WA, 98032, USA

Precision landing is a key requirement for sustainable lunar surface access. Active precision navigation is a critical technology that satisfies this requirement. It enables lunar vehicles to autonomously "land anywhere, land anytime" without suffering from limitations encountered by passive approaches. This paper details the rapid maturation of an active Terrain Relative Navigation (TRN) system which is comprised of sensing and processing components, both of which build on proven flight heritage origins. This active TRN system has been flight tested on a fixed-wing platform for risk reduction of the technology prior to inclusion on upcoming lunar missions. This flight testing included the first real-time demonstration of the active TRN system. Results from these test campaigns are presented to show that the active TRN capability can satisfy precision landing accuracy requirements.

I. Introduction

Since the inception of the NASA Artemis program, a precision landing requirement has existed for missions to the lunar surface [1]. Both crewed and uncrewed missions under the Human Landing System (HLS) and Commercial Lunar Payload Services (CLPS) programs mandate autonomous precision landing as a key requirement. This requirement drives the need for an onboard navigation system to provide state knowledge with enough precision to enable landing accuracy within 50 m of a targeted site.

Various navigation approaches exist to meet the precision landing requirement, but for initial missions to the Moon where other navigation aids are unavailable, Terrain Relative Navigation (TRN) is the enabling technology. All TRN systems function in the same basic manner: observations of the terrain surface are autonomously compared against reference data to determine a navigation state. Recent examples of successful TRN applications for precision landing include the OSIRIX-REx and Mars2020 landings [2,3]. TRN capabilities have also been developed for demonstration and utilization on upcoming lunar missions [4,5] and other interplanetary applications [6,7].

The principal limitation of these approaches is that they rely on sensing via passive optical cameras. While mature and flight proven, the downside of any passive approach is that the TRN sensor can only be used when the terrain surface is visible. This limitation places a constraint on landing site selection, approach trajectory, and landing time. Active TRN circumvents this limitation by sensing the terrain surface independently from illumination conditions. The basic active TRN concept, utilizing various active sensing technologies, has historically existed for terrestrial GPS-denied navigation applications and has been previously proposed for application to lunar missions [8-10].

Blue Origin has been developing and testing lunar guidance, navigation, and control capabilities and through the NASA Deorbit, Descent, and Landing (DDL) Tipping Point program, two suborbital test flights were performed using the New Shepard vehicle [11]. These flights included a suite of technologies, and findings from the test campaign have informed the development of the LiDAR sensor described in this paper. Additionally, core navigation algorithms and software were also developed and demonstrated under this program. Following the completion of the partnership, private development of an active LiDAR-based TRN system was initiated to address the emergent limitations of passive TRN.

[1] Senior GNC Engineer, Advanced Development Programs.
[2] GNC Engineer, Advanced Development Programs.
[3] Senior GNC Engineer, Advanced Development Programs.
[4] Senior Technical Fellow, Advanced Development Programs, AIAA Senior Member.

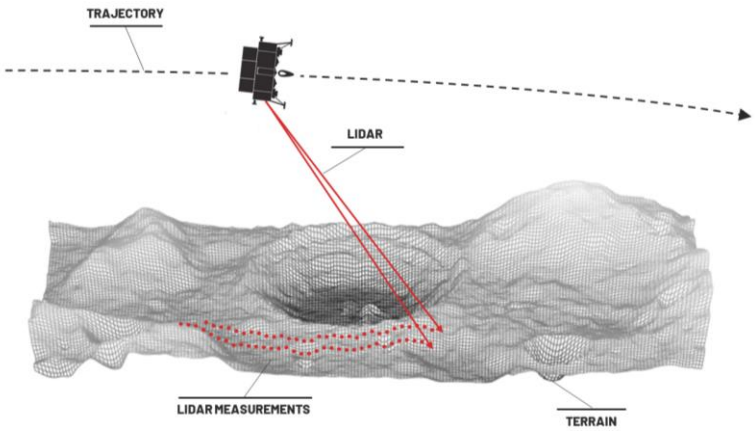

Fig. 1 Active TRN Concept-of-Operations

The TRN approach that is illustrated in Fig. 1 makes use of a multi-beam LiDAR rangefinder which serves as the active sensor. Discrete range measurements between the sensor and lunar surface are used to provide the data needed for TRN processing. Section II of this paper provides further technical detail regarding this approach and shows analysis of predicted performance. To rapidly mature this active TRN technology for application on upcoming lunar missions, terrestrial fixed-wing flight testing has been performed. Section III details these flight campaigns and results from this testing are presented in Section IV.

II. Technology Overview

The active TRN system described in this paper is comprised of a sensing component and a processing component as shown in Fig. 2. The sensing component collects measurements of the terrain surface, and the processing component compares these measurements with onboard map data to provide a navigation solution. Both components are detailed in this section along with corresponding analysis that shows the predicted performance of the integrated system. Though the specific lunar application of this concept is novel, the fundamental technology that active TRN builds upon is relatively mature and well understood.

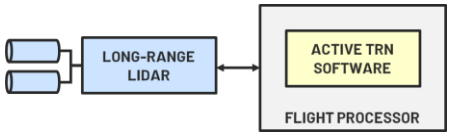

Fig. 2 Active TRN System Components

A. Algorithm Overview

There are multiple algorithmic approaches for performing active TRN. Several methods have been investigated and evaluated against criteria consisting of navigation performance, resource requirements, and complexity. This evaluation has led to the selection of a profile matching algorithm as the baseline approach for the active TRN in this paper. The major functional components of this approach are outlined in Fig. 3 (not shown are various stages of outlier rejection employed throughout the data processing pipeline for robustness).

The profile matching algorithm relies on accumulating LiDAR range measurements over an interval of time and combining them with an estimated navigation state to form a terrain profile. A matching operation is then performed between the measured profile and known reference terrain to produce a three-dimensional position offset. A formulation of normalized cross-correlation is employed to efficiently determine this offset with invariance to magnitude and data sparsity differences between measured profiles and reference terrain data. The profile match offset represents error in the estimated navigation state and forms the TRN update used to correct this error.

This algorithm achieves the navigation performance needed while also satisfying computational resource and complexity criteria. A similar algorithmic approach has been detailed by JPL [12] and utilized for independent verification and validation of the Blue Origin active TRN system.

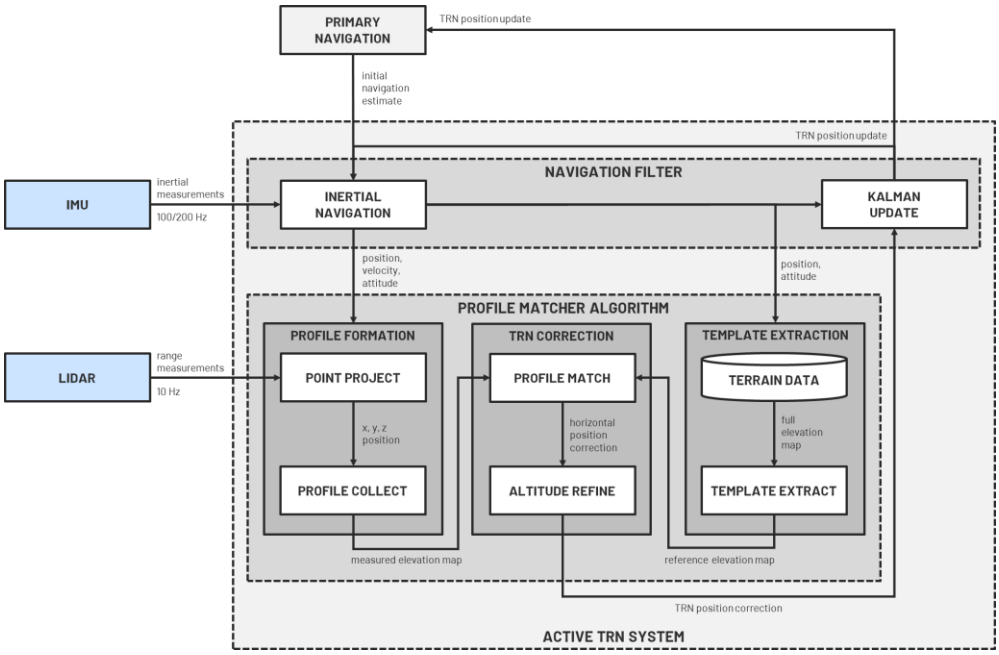

Fig. 3 Active TRN Algorithm

B. Sensor Overview

Utilizing the profile matching algorithm, sensitivity studies have been conducted to inform driving sensor requirements needed to perform active TRN. Numerous factors such as range, noise, beamwidth, etc. were analyzed to establish high-level sensor specifications (see Table 1). The primary driving requirement is the measurement range needed to provide active TRN coverage prior to powered descent initiation and through to landing. This requirement must accommodate a diversity of landing sites and approach trajectories. The number of beams providing range measurements is another important requirement. While active TRN can be achieved with only a single beam, additional beams oriented in different directions increase the overall system fault tolerance and improve availability by increasing the probability of observing dense terrain features (the profile matching algorithm is formulated in a manner that accommodates additional data sources from multiple beams in a computationally efficient manner).

Table 1 LoRA Specifications

Line-of Sight Measurement Range	1 – 30 km
Line-of-Sight Measurement Accuracy	≤ 1 m (3σ)
Line-of-Sight Velocity Limits	± 400 m/s
Number of Beams	2
Measurement Rate	10 Hz
Beam Divergence	≤ 0.025 deg (half-angle)

An additional consideration is sensor maturity and the path to operational flight use. The sensor under development for active TRN is called the Long-Range Altimeter (LoRA). The LoRA is developed by Optical Air Data Systems and is a derivative of the flight-proven Optical Moon Proximity Sensor (OMPS). The OMPS was originally developed for lunar application and has been flight tested on New Shepard in 2020 and 2021 under the Tipping Point program [11]. The OMPS provides discrete range and velocity measurements from four optical heads, whereas the LoRA (shown in Fig. 4) has extended range and only two optical heads. The principal advantage of this sensor strategy is the rapid development awarded by iterating upon an existing design with spaceflight heritage.

Fig. 4 LoRA Optical Telescopes and Electronics Chassis

C. Lunar Analysis

A framework for analysis and test of this active TRN system has been developed. LiDAR measurements are provided from a sensor model that performs ray-terrain intersection to accurately predict range values given position, velocity, and attitude information. All sensor parameters are modeled, and system-level errors such as beam line-of-sight misalignment are also included. Multiple lunar terrain data sets are utilized to test the system performance in simulation. From a TRN perspective, lunar maria terrain is used to capture flat feature-sparse regions, and lunar highlands terrain is used to capture rough feature-dense regions. As the performance of the TRN system is terrain dependent, map data from each of these regions is used to provide a comprehensive representation of the lunar environment (see Fig. 5).

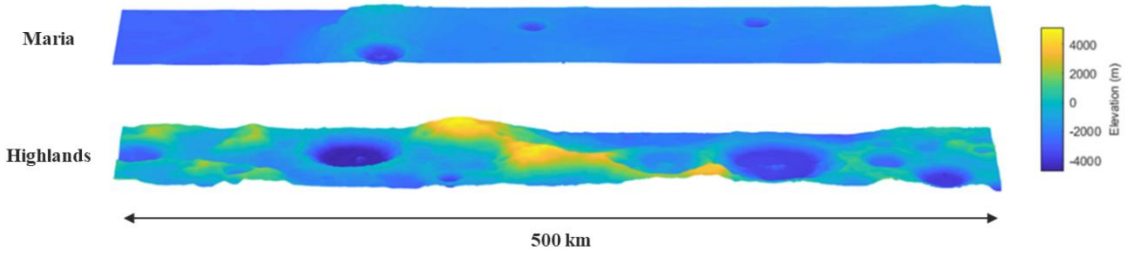

Fig. 5 Lunar Terrain Data Sets

The performance of the TRN system is fundamentally driven by the resolution of the reference terrain data (with higher spatial resolution providing greater profile match accuracy). Reference terrain data is split into multiple discrete maps that provide continuous ground coverage with increasing resolution during the lunar descent. A progression from 60 m/px to 5 m/px has been utilized and data has been sourced from the Lunar Reconnaissance Orbiter Laser Altimeter (LOLA) [13] and Kaguya Terrain Camera (TC) [14]. Synthetic craters were added to the terrain data used by the LiDAR model to represent features that will be seen by the sensor during landing but are not present in the reference data due to resolution limitations (the terrain data used by the active TRN algorithm is left unmodified).

Monte Carlo analysis has been performed using the active TRN flight software against both maria and highlands data sets with the high-level initial conditions listed in Table 2. Closed-loop analysis has been performed with vehicle-level guidance and control, but open-loop analysis against a set of dispersed trajectories allows for navigation performance to be observed separately. See Fig. 6 for open-loop results where the system can be seen showing closure against the 50 m precision landing requirement at landing. Additionally, note that differences in the final position error achieved between the different types of terrain are minimal. This is critical as it illustrates the generalized performance of the algorithm across the diversity of lunar terrain types and demonstrates the global availability of the active TRN system. Similar results have been obtained by independent, external analysis [10,12].

Table 2 Monte Carlo Initial Conditions

Position Knowledge Error (3σ)	[1500, 5000, 1000] m (radial, in-track, and cross-track)
Velocity Knowledge Error (3σ)	[4.0, 1.0, 0.5] m/s (radial, in-track, and cross-track)
Attitude Knowledge Error (3σ)	[0.15, 0.15, 0.15] deg (per-axis)

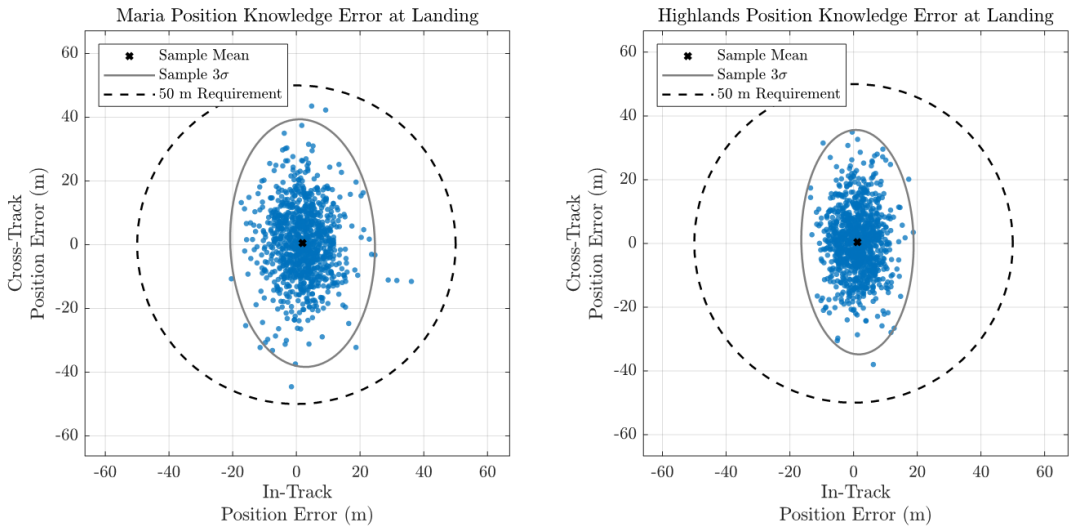

Fig. 6 Active TRN Monte Carlo Results (1000 Runs)

Sensitivity studies have also been performed using this analysis framework. Factors that contribute to active TRN performance are knowledge initialization error, profile length, minimum altitude/velocity, and reference map resolution:

- The TRN system is specifically designed to correct position error and is therefore insensitive to position knowledge at initialization. The only implication is the sizing of reference terrain data, and this can be addressed through mission planning and incorporation of expected uncertainty. Velocity knowledge at initialization can impact profile formation, but for the lunar mission scenario these errors are not significant. The primary driver for active TRN performance is attitude knowledge at initialization (and beam pointing knowledge more broadly). Analysis has shown a graceful degradation in performance as greater pointing errors lead to greater position bias in the TRN corrections. This effect is greater at high altitude and is minimized during the natural progression toward the lunar surface during powered descent. The incorporation of a star tracker is assumed at the vehicle level for this active TRN system.
- The profile length is selected to balance several factors. Greater accuracy and robustness to ambiguity can be achieved with a longer profile. However, a longer profile results in greater susceptibility to velocity error over the measurement interval as well as a more infrequent TRN update rate. Intervals on the order of 5 sec have been found to strike a balance between these considerations.
- The lower limit for active TRN operation is dependent on several factors and is sensitive to differences in the terminal landing trajectory and sensor orientation. Fundamentally, this constraint arises when profiles can no longer be formed and matched by active TRN. The system is designed to nominally stop operation at a range of 1 km to the landing site.
- Spatial resolution of reference map data is a driver for any form of TRN system. While higher resolution increases precision, lower resolution allows for faster computation and reduced storage needs. Therefore, the progression from 60 m/px to 5 m/px has been selected along the powered descent and landing profile. This allows requirements to be satisfied with lunar terrain data that is available for operational use.

The active TRN flight software is implemented in C/C++ and has been deployed to flight avionics hardware for processor-in-the-loop demonstration and testing. Profiling has shown that active TRN corrections can be computed at an update rate that is less than the LiDAR profile collection interval. Analysis has shown that this measurement rate is more than sufficient to meet precision landing requirements.

III. Flight Test Overview

Two flight campaigns were executed in 2022 to further mature the active TRN technology. Test objectives included demonstration of sensor and flight software functionality as well as validation of simulation assumptions to anchor lunar performance. The first test was primarily a data collection effort that utilized the OMPS sensor while construction of the LoRA was taking place. The second test incorporated the newly built LoRA (Fig. 7) and also featured real-time onboard demonstration of the active TRN flight software. The second test was funded by NASA as a technology risk reduction for HLS.

The campaigns were conducted on a Gulfstream III jet platform that provided the necessary altitude and ground speeds needed to perform the flight testing in a representative manner. Two main test profiles were utilized for each campaign. Racetrack profiles were collected at a constant altitude and ground speed and were used to maximize data collection efficiency. Surrogate lunar descent profiles were also used to capture mission representative data that matched the final portion of a lunar descent trajectory as closely as practical. Ground speeds ranged from 0 – 200 m/s and altitudes ranged from 0 – 8 km (above ground level). The LiDAR sensors were mounted in a centerline fairing with fixed line-of-sight to the terrain surface. Additionally, a tactical-grade INS was utilized to provide a truth trajectory and raw IMU measurements for active TRN processing. All sensors were installed in a common mechanical bracket assembly within the centerline fairing. This assembly also contained an air anti-fogging system and a witness camera to confirm unimpeded optics for the duration of flight operations. Data collection equipment and engineering displays were installed in the cabin and on the second campaign the active TRN flight processor was also installed. Integration and test of all components and a brief checkout flight were conducted prior to execution of each campaign.

Fig. 7 LoRA Engineering Unit, Sensor Fairing, Testbed Aircraft, and In-Cabin Engineering Station

Flights were conducted in two major geographic areas in Texas (TX) and Wyoming (WY). Both test locations contained different terrain types which were broadly categorized as either feature-dense or feature-sparse (see Fig. 8). The feature-dense terrain contained significant relief and was analogous to lunar highlands terrain while the feature-sparse terrain was flatter and analogous to lunar maria. In either case, flight profiles were collected over areas devoid of significant vegetation and non-natural features. Reference terrain data was sourced from the USGS 3D Elevation Program (3DEP) [15] and reformed for active TRN utilization at spatial resolutions of 8 – 9 m/px.

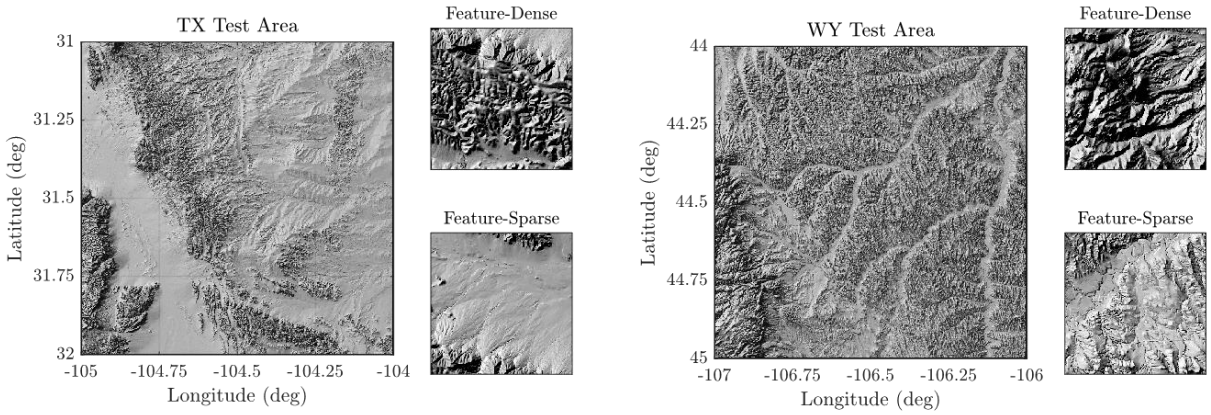

Fig. 8 Terrestrial Flight Test Terrain in TX and WY

As previously mentioned, during the second test campaign, the active TRN system was operated onboard. Data from the LoRA was sent to a flight processor which executed the profile matching software against terrain maps covering the test areas. This was the first real-time demonstration of the fundamental algorithm in a flight environment. Live demonstration also served as a validation of several processes that are key drivers of system performance. Pre-flight metrology was performed to characterize the as-installed LiDAR beam line-of-sight angles. This drives TRN performance as error in pointing knowledge manifests as a position bias in the output from the TRN algorithm. The terrain map formation process also presents a bias source as any error in the georegistration of the reference terrain data is directly carried as an error in the TRN position solution. Categorization of in-flight system performance has shown that these error sources can be kept within the needed tolerances to meet position accuracy requirements.

Approximately 15 total hours of flight testing were performed across both campaigns (see Table 3 for a summary of test points). Each test point varied the altitude, ground speed, heading, or terrain type to capture a diverse, lunar representative data set. The lunar operating time for active TRN is only a few minutes to provide precision navigation during powered descent and landing and therefore there is a significant amount of terrestrial data now available for performance analysis.

Table 3 Summary of Collected Data

Campaign #1 *OMPS Only*	25 racetrack profiles	5 surrogate profiles	30 total test points	7.5 total flight hours
Campaign #2 *LORA & OMPS*	16 racetrack profiles	7 surrogate profiles	23 total test points	7.5 total flight hours

IV. Flight Test Results

All results presented in this section are from the second test campaign and are exclusive to performance provided by the LoRA sensor. The results are discussed at the sensor-level, algorithm-level, and system-level.

A. Sensor Performance

First presented is an analysis of the difference between raw LoRA range measurements and predictions from the sensor model. The purpose of this analysis is to confirm that the sensor is satisfying specified requirements and to validate the model. This validation is important because the sensor model is utilized for lunar simulation and performance analysis. As shown in Fig. 9, the difference between the measurements and predictions is minimal and within expectations. Residual differences are attributable to uncorrected pointing knowledge error and uncertainty in the reference elevation data that is utilized for the ray-terrain intersection.

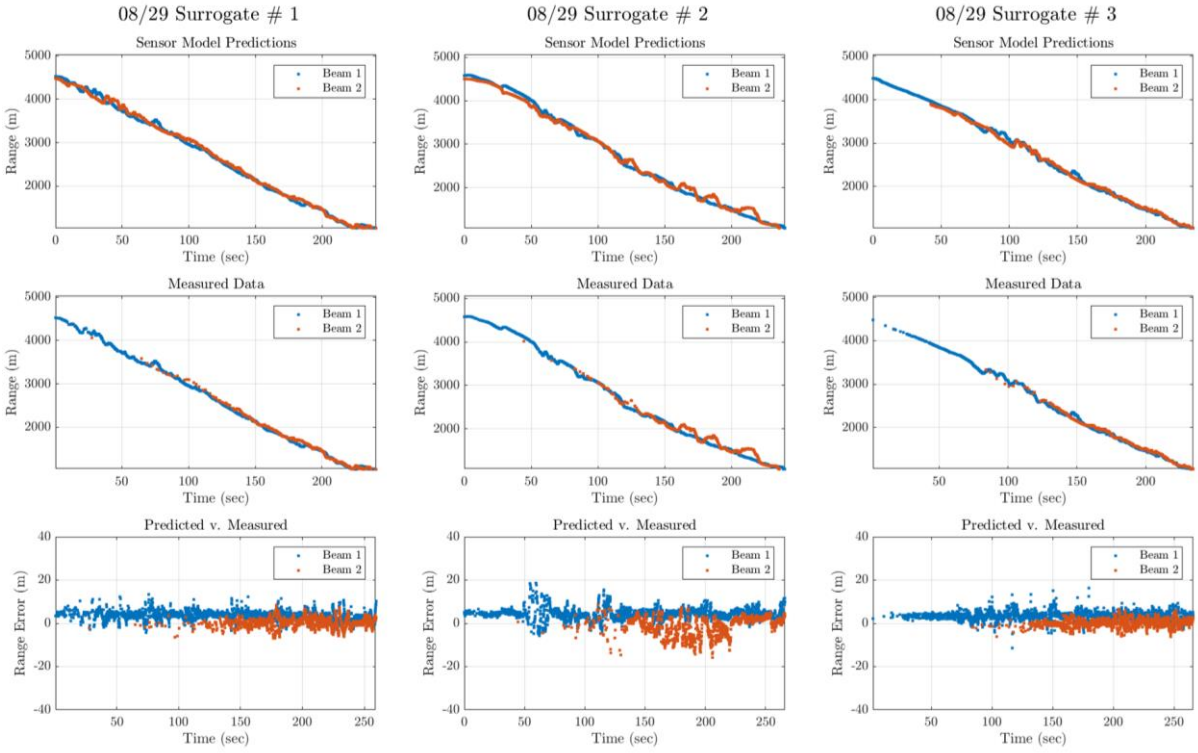

Fig. 9 Raw LoRA Range Measurements and Sensor Model Predictions

Sensor performance was also compared against data from the GSFC Land, Vegetation, and Ice Sensor (LVIS) LiDAR [16]. Specific grounding runs were collected between waypoints previously surveyed by LVIS, enabling additional validation of sensor functionality.

B. Profile Matcher Algorithm Performance

Following a grounding of the raw sensor performance, attention can be turned to the core profile matching algorithm. See Fig. 10 for a summary of total position error from this algorithm across all collected test points (separated by terrain type). There are over 1000 samples present in this plot with each sample consisting of the error between a given TRN correction and the truth trajectory. Factors that contribute to this error include the performance of the profile matching algorithm itself as well as bias from beam pointing knowledge, terrain data geolocation, and time synchronization of sensor data.

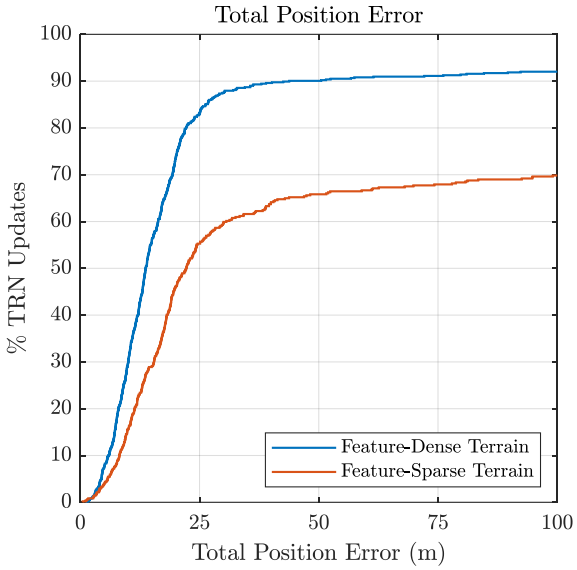

Fig. 10 Total Position Error of Profile Matcher Algorithm

Two key performance metrics illustrated by this plot are the algorithm accuracy and availability. Accuracy is defined as the amount of position error and is observable on the x-axis. It is the most important metric as it drives the overall performance of the active TRN system. Availability is the ability for the profile matcher to return a position fix for a given interval of time and is observable on the y-axis. Unlike accuracy, this can be addressed at the system-level by coasting inertially during periods where the profile matching algorithm fails to produce a solution.

The results show that approximately 90% of all profile matches on feature-dense terrain exhibit position error less than 50 m. The feature-sparse terrain reduces availability, but the accuracy of the profile match output is still sufficient for use at the active TRN system-level (e.g. 65% of total position error is less than 50 m). The objective of the test campaign was to collect data at a diversity of conditions, and the challenging feature-sparse terrain provides an important mechanism to determine where profile matching availability is reduced. Recall that results were generated in real-time during flight test operations and no further optimization of beam alignment has been performed. The results reflect the real-world operation of the active TRN system, and this performance validates the results obtained from lunar simulations of the active TRN system.

To better understand bias sources, see Fig. 11 for the horizontal position error of these profile matcher results. Note that these results differ from those shown in Fig. 6 as they are error in the core algorithm, not the final position error at the end of a landing run (the results in Fig. 6 have also been processed by the active TRN navigation filter which further improves the precision of the profile matcher).

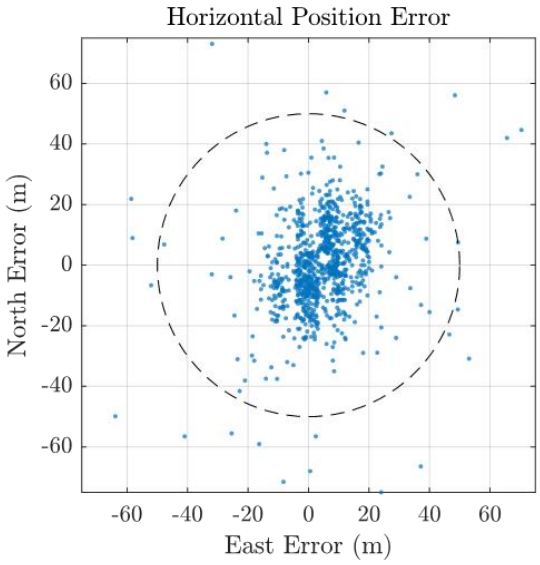

Fig. 11 Horizontal Position Error of Profile Matcher Algorithm

The non-uniformity of the horizontal error is a result of flight profiles being repeatedly conducted between waypoints with the same ground track. The profile matching algorithm is inherently more accurate in the in-track direction of travel compared to the cross-track direction due to density of measurements produced along the vehicle flight path (this same phenomenon is observable in the lunar simulation results shown in Fig. 6). Performance for each test point is summarized in Table 4 and Table 5. Racetrack profiles are denoted with "R" and surrogate profiles are denoted with "S". Each test point has a different altitude, ground speed, and heading. Performance is relatively invariant to these factors and only the terrain type is listed. Availability is the percentage of samples that result in a returned TRN correction from the profile matcher algorithm. For these results, accuracy is presented as the horizontal Circular Error Probable (95%) of TRN corrections conditional on availability.

Table 4 TX Profile Matcher Performance

Test Point	Terrain	Samples	Availability	Accuracy *CEP95*
R1	Sparse	58	58.62 %	40.71 m
R2	Dense	61	93.44 %	21.28 m
R3	Sparse	43	39.53 %	46.87 m
R4	Dense	68	79.41 %	28.16 m
R5	Dense	55	92.73 %	35.51 m
R6	Sparse	57	49.02 %	29.13 m
R7	Dense	64	96.88 %	19.78 m
R8	Sparse	41	92.68 %	38.83 m
R9	Sparse	59	29.31 %	36.51 m
R10	Dense	59	88.14 %	26.68 m
S1	Dense	51	94.12 %	24.83 m
S2	Dense	53	79.25 %	21.21 m
S3	Dense	48	81.13 %	21.52 m

Table 5 WY Profile Matcher Performance

Test Point	Terrain	Samples	Availability	Accuracy *CEP95*
R1	Dense	45	100.00 %	17.96 m
R2	Sparse	55	90.74 %	28.15 m
R3	Dense	48	87.50 %	20.67 m
R4	Sparse	44	65.31 %	27.67 m
R5	Dense	48	93.75 %	29.75 m
R6	Sparse	50	92.00 %	29.62 m
S1	Dense	23	100.00 %	24.95 m
S2	Sparse	42	89.19 %	39.44 m
S3	Dense	40	95.00 %	30.30 m
S4	Sparse	34	63.64 %	39.58 m

C. Integrated System Performance

With an understanding of the core profile matching algorithm performance, the active TRN system-level performance is now presented with respect to navigation requirements (i.e. maintaining position error less than 50 m over time to enable precision landing). In order to operate on the flight data, the only configuration changes made to the active TRN system are the gravity model used for Earth operation and characteristics for the tactical-grade MEMS IMU that was utilized. The navigation filter is otherwise untuned for this terrestrial data.

The horizontal and vertical components of position error are shown in the bottom row plots of Fig. 12 for surrogate profiles that were conducted to match that of a lunar descent. The altitude profiles and displayed in the top row to provide context for the trajectory, and range data from the LoRA is displayed in the top row of plots to provide context for the measurements the active TRN system is consuming. At the beginning of each run, the active TRN system is initialized with position, velocity, and attitude information. From this point onward, the active TRN system only consumes IMU measurements and range data from the LiDAR.

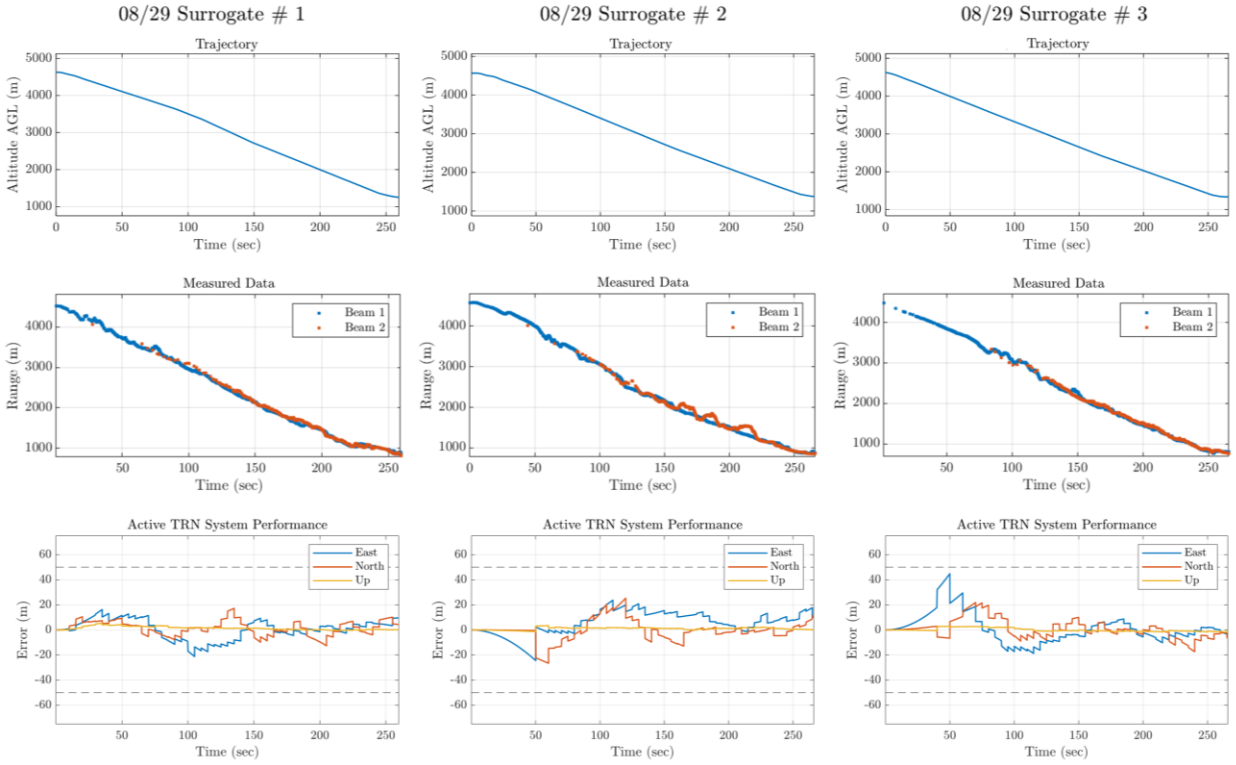

Fig. 12 Active TRN System-Level Performance on Surrogate Lunar Descents

Multiple minutes of operation are shown in these plots over representative flight profiles and representative terrain. The vertical component of position error is unsurprisingly very low, and the horizontal error component remains within the 50 m requirement for each run.

The effect of the profile matcher availability is noticeable in these results. Observe the active TRN behavior at the beginning of run #2 (center) and run #3 (right) where sensor data is limited at long range. During this time, the profile matcher is unable to produce TRN corrections and the position error of the navigation filter grows while coasting inertially. Once availability is obtained, the position error is immediately reduced and continues to stay within expectations until the end of a run. This is notable as it shows the inherent robustness of the active TRN system to data sparsity/sensor faults.

V. Conclusion

The purpose of the flight testing detailed in this paper was to mitigate the developmental risk in the active TRN technology. At the conclusion of this testing, the viability of the active TRN navigation approach in addressing NASA landing accuracy requirements has been flight proven. A new sensor has been developed and functionally validated. The profile matching algorithm has been demonstrated in real-time on a flight processor. Finally, the active TRN system as a whole has been exercised with lunar representative flight trajectories and lunar representative terrains. The active TRN system was shown to be capable of providing a navigation solution with position error within 50 m across a diversity of test points and on surrogate lunar descents. Major developmental risks have been retired and the active TRN system is showing closure against requirements for precision lunar landing. Continued verification and validation testing of this active TRN system is ongoing prior to lunar application.

Acknowledgments

The authors would like to acknowledge Optical Air Data Systems for development of the LoRA sensor and the Calspan Corporation for providing the test aircraft. The authors would also like to acknowledge Kyle Hickman, Allison De Larosiere, Daniel Brun, and Michael Andrle for their contributions during flight testing. The development of the active TRN system described in this paper has been privately funded by Blue Origin. The second test campaign was partially funded by NASA contract 80MSFC21CA015 for NextSTEP-2 Appendix N CLIN002-Task005.

References

[1] Chavers, G., Watson-Morgan, L., Smith, M., Suzuki, N., and Polsgrove, T., "NASA's Human Landing System: The Strategy for the 2024 Mission and Future Sustainability," *IEEE Aerospace Conference*, 2020. doi: 10.1109/AERO47225.2020.9172599

[2] Lorenz, D., Olds, R., May, A., Mario, C., Perry, M., Palmer, E., and Daly, M., "Lessons Learned from OSIRIS-Rex Autonomous Navigation Using Natural Feature Tracking," *IEEE Aerospace Conference*, 2017. doi: 10.1109/AERO.2017.7943684

[3] Johnson, A. et al., "Mars 2020 Lander Vision System Flight Performance," *AIAA SciTech Forum*, 2022. doi: 10.2514/6.2022-1214

[4] Owens, C. et al., "Development of a Signature-based Terrain Relative Navigation System for Precision Landing," *AIAA SciTech Forum*, 2021. doi: 10.2514/6.2021-0376

[5] Marshall, J., "Intuitive Machines Unveils 2021 Moon Landing Navigation Approach," Intuitive Machines Press Release, 2020.

[6] Witte, I., Bekker, D., Chen, M., Criss, T., Jenkins, S., Mehta, N., Sawyer, C., Stipes, J., Thomas, J., "No GPS? No Problem! Exploring the Dunes of Titan with Dragonfly Using Visual Odometry," *AIAA SciTech Forum*, 2019. doi: 10.2514/6.2019-1177

[7] Trawny N., Katake, A., Cheng, Y., Conway, D., San Martin, M., Skulsky, D., Johnson, A., "The Intelligent Landing System for Safe and Precise Landing on Europa," *AAS Guidance, Navigation and Control Conference*, 2017.

[8] Johnson, A., and Montgomery, J., "Overview of Terrain Relative Navigation Approaches for Precise Lunar Landing," *IEEE Aerospace Conference*, 2008. doi: 10.1109/AERO.2008.4526302

[9] Johnson, A., and Ivanov, T., "Analysis and Testing of a LIDAR-Based Approach to Terrain Relative Navigation for Precise Lunar Landing," *AIAA Guidance Navigation and Control Conference*, 2011. doi: 10.2514/6.2011-6578

[10] "Human Landing System (HLS) Program White Paper Active Terrain Relative Navigation for Sustained Lunar Landing," NASA HLS-PAP-025, 2022.

[11] Bieniawski, S., Lewis, B., Friia, B., Mahajan, A., Somervill, K., Priyavadan, M., and Dakin, D., "New Shepard Flight Test Results from Blue Origin De-Orbit Descent and Landing Tipping Point," *AIAA SciTech Forum*, 2022. doi: 10.2514/6.2022-1829

[12] Chen, P. T., Johnson, A., Setterfield, T., Katake, A., Cheng, Y., Griffin, G., "Active Terrain Relative Navigation for Lunar Landings," *AAS Guidance, Navigation and Control Conference*, 2022.

[13] Neumann, G.A., "2009 Lunar Orbiter Laser Altimeter Raw Data Set," LRO-L-LOLA-4-GDR-V1.0, NASA Planetary Data System, 2010. doi: 10.17189/1520642

[14] Barker, M. K., Mazarico, E., Neumann, G. A., Zuber, M. T., Haruyama, J., and Smith, D. E., "A new lunar digital elevation model from the Lunar Orbiter Laser Altimeter and SELENE Terrain Camera," *Icarus*, Vol. 273, 2016, pp. 346-355. doi: 10.1016/j.icarus.2015.07.039

[15] U.S. Geological Survey, "1/3rd arc-second Digital Elevation Models (DEMs)," USGS National Map 3DEP Downloadable Data Collection, 2017.

[16] Blair, B., Rabine, L., Hofton, M., "The Laser Vegetation Imaging Sensor: A medium-altitude, digitisation-only, airborne laser altimeter for mapping vegetation and topography," *ISPRS Journal of Photogrammetry & Remote Sensing*, Vol. 54, pp. 115-122. doi: 10.1016/S0924-2716(99)00002-7